Journal of Alloys and Compounds 981 (2024) 173708

Contents lists available at ScienceDirect

Journal of Alloys and Compounds

journal homepage: www.elsevier.com/locate/jalcom

Exploring the impact of rare-earth (La^{3+}) ions doping on structural, magnetic, and dielectric properties of $Co_{0.50}Ni_{0.50}La_xFe_{2-x}O_4$ nano-spinel ferrite

K. Sakthipandi [a,*], K. Venkatesan [a], R. Sivakumar [b], G. Rajkumar [b], B. Ganesh Babu [c], S. Arunmetha [d], Aslam Hossain [e], M. Srinidhi Raghavan [f], V. Rajendran [g]

[a] Department of Physics, SRM TRP Engineering College, Tiruchirappalli 621 105, Tamil Nadu, India
[b] Department of Physics, Easwari Engineering College, Chennai 600 089, Tamil Nadu, India
[c] Department of Mechanical Engineering, SRM TRP Engineering College, Tiruchirappalli 621 105, Tamil Nadu, India
[d] Centre for Advanced Energy Studies, Department of Electronics and Communication Engineering, Koneru Lakshmaiah Education Foundation, Guntur, Andhra Pradesh 522 302, India
[e] Smart Materials Research Institute, Southern Federal University, Sladkova 178/24, 344090 Rostov-on-Don, Russia
[f] Department of Chemistry and Centre for Nano, Materials and Displays, B.M.S. College of Engineering, Bengaluru 560 019, Karnataka, India
[g] Centre for Nanotechnology, Academy of Maritime Education and Training (Deemed to be University), Chennai 603 112, Tamil Nadu, India

ARTICLE INFO

Keywords:
$Co_{0.50}Ni_{0.50}La_xFe_{2-x}O_4$ spinel ferrites
Structural properties
Ultrasonic velocity
Magnetic measurements
Blocking temperature
Curie temperature

ABSTRACT

This study used a sonochemical reactor to synthesize $Co_{0.50}Ni_{0.50}La_xFe_{2-x}O_4$ ($0.00 \leqslant x \leqslant 0.2$; step 0.05) spinel ferrites. X-ray diffraction spectra and scanning electron microscope (SEM) images were employed to verify and authenticate the physical characteristics, such as crystalline structure and morphology of the $Co_{0.50}Ni_{0.50}La_xFe_{2-x}O_4$ spinel ferrite particles. These structural analyses are targeted to confirm the singular-phase cubic Fd-3 m spinel ferrite nature. It has been noted from the SEM images that every particle resembles a sphere-like morphology. The real dielectric constants and dielectric loss of the prepared $Co_{0.50}Ni_{0.50}La_xFe_{2-x}O_4$ spinel ferrites were measured. The blocking (T_B) and Curie (T_C) temperatures of the spinel ferrites can also be explored and measured using temperature-dependent susceptibility and ultrasonic non-destructive techniques (NDT), respectively. The difference between the T_B and T_C is quite small. This observed difference implies that finding the phase transition temperature of spinel ferrites using ultrasonic NDT testing is a more flexible process than any other conventional technique. The room-temperature hysteresis shows that these La^{3+} doped $Co_{0.50}Ni_{0.50}La_xFe_{2-x}O_4$ ferrite samples might be more suitable for applications.

1. Introduction

In the past two decades, many scientists have been concerned/interested in studying the relationships between compositional and structural factors and the magnetic and electric properties of spinel ferrite nanoparticles [1–3]. Spinel ferrites, such as magnetite, excel in magnetic recording, while garnet ferrites are preferred for their low magnetic loss at high frequencies in microwave devices. Hexagonal ferrites find common use in permanent magnets, and mixed metal ferrites can be customized for specific purposes based on their composition [4]. Recent studies showcase the remarkable utility of spinel ferrites in various applications such as catalysts, gas sensors, magnetic drug delivery systems, rechargeable lithium batteries, information storage, magnetic cores, adsorbents, magnetic fluids, microwave absorbers, and medical diagnostics [5,6]. The ferrite structure comprises two types of metal ions (A and B) arranged in A-O tetrahedra and B-O octahedra, typically represented by the general chemical formula AB_2O_4 [7]. Spinel materials are primarily divided into three groups, including conventional spinel, inverse spinel, and complex spinel, based on the distribution of divalent metal ions and Fe^{3+} on the two cationic sites. Researchers are particularly interested in spinel ferrites because of their intriguing magnetic, electrical, and optical properties [8]. The exceptional accomplishments are attributed to attributes like elevated saturation magnetization, minimal coercivity, a higher Curie temperature (T_C), and substantial electric resistivity, among other factors. Spinel ferrites, owing to their diverse composition, valence states, and electron

* Corresponding author.
E-mail address: sakthipandi@gmail.com (K. Sakthipandi).

https://doi.org/10.1016/j.jallcom.2024.173708
Received 15 December 2023; Received in revised form 14 January 2024; Accepted 28 January 2024
Available online 1 February 2024

configurations, inherently possess magnetic, electrical, optical, and catalytic capabilities [9,10].

For practical applications, the enhanced and controlled properties of spinel ferrites are achieved by (i) co-doping the metal ion (A-site) with other divalent metals ions (Ni^{2+}, Cu^{2+}, Zn^{2+}, and Co^{2+}) and (ii) co-doping the Fe-site with other trivalent elements (Cr^{3+}/Al^{3+}) or rare-earth elements (La^{3+}/Er^{3+}). The features/applications of this co-doped ferrite system depend critically on the re-distribution/arrangement of cations at the tetrahedral site (A-site) and the octahedral site (B-site) [11–17]. These co-doping spinel ferrites have a variety of magnetic, electrical, and optical properties [16–19]. Several synthetic co-doping at A-site and Fe-site have recently made it possible to create new materials with desired magnetic characteristics suitable for specific applications [11–19]. In this apprehension, the Li-Ni [20], Ni-Cu-Zn [21], Co-Ni [22], Ni-Zn-Mn [23] Li-Co [24], Co-Cr [25], Zn-Co [26], Cd-Co [27], Mg-Zn [28] and other ferrites were synthesized and thoroughly examined to enhance the properties of the base materials. These investigations aimed to uncover distinct electrical, magnetic, and X-band shielding characteristics. Based on the literature review, this study aims to study cobalt-nickel ferrites. For half-codoped $Ni_{0.5}Co_{0.5}Fe_2O_4$ ferrite, a higher capacitance value of 865 Fg^{-1} is reported [29].

In spinel ferrites, nickel tends to favor the B-site, whereas cobalt and iron ions commonly occupy both the A- and B-sites. The ratio of occupation can significantly shift with changes in crystallite size. Cobalt, known for its robust magnetic properties, exhibits high coercivity, excellent chemical and physical stability, substantial anisotropy, and moderate magnetization. These characteristics make cobalt valuable in spinel ferrites, contributing to their overall magnetic behavior and stability. Therefore, cobalt ferrite has its own uses for information storage, audio/video tapes, high-density digital recording disks, and magnetic recording technology [30]. On the other hand, nickel ferrite is a soft magnetic material because of its smaller magnetic moment and weaker magneto-crystalline anisotropy. However, Ni^{2+} reduces the coercivity of Co^{2+} ferrite. Additionally, it is evident that the alternate current (ac) electric and magnetic losses are reduced by partially substituting Ni for Co [31,32]. The dissimilarity of conductivity dependence on frequency heavily hinges on the balance between hard and soft spinel ferrite compositions.

Further, the electrical and magnetic characteristics of ferrites and oxides undergo significant alterations upon introducing trivalent ions, rare-earth ions, or a combination of both in place of the Fe^{3+} ion. The primary objective behind substituting Fe ions with La is to heighten the electrical resistivity of spinel ferrites. This targeted enhancement becomes pivotal in minimizing electrical or dielectric losses, especially in applications operating at high frequencies. These co-doped spinel ferrites exhibit small dielectric loss, which is suitable for high-frequency applications. Various techniques, including sol-gel, auto-combustion, co-precipitation, hydrothermal synthesis, and sonochemical reactions, have been employed for the production of nano-sized spinel ferrite particles. Sonochemical methods, in particular, yield nanoparticles characterized by high uniformity in size and composition, thereby enhancing the material properties. The application of ultrasonic waves in this process improves the crystallinity, surface activity, and overall performance of the synthesized nanoparticles [33–37]. This study used the sonochemical reaction approach to synthesize La-doped cobalt--nickel ferrite $Co_{0.50}Ni_{0.50}La_xFe_{2-x}O_4$ (CNLFO; $0.00 \leqslant x \leqslant 0.2$; step 0.05) powders. This work has explored how La substitution affects the structural, magnetic, and electric properties of the prepared $Co_{0.5}Ni_{0.50}Fe_2O_4$ (CNLFO00), $Co_{0.5}Ni_{0.50}La_{0.05}Fe_{1.95}O_4$ (CNLFO05), $Co_{0.5}Ni_{0.50}La_{0.10}Fe_{1.90}O_4$ (CNLFO10), $Co_{0.5}Ni_{0.50}La_{0.15}Fe_{1.85}O_4$ (CNLFO15), and $Co_{0.5}Ni_{0.50}La_{0.20}Fe_{1.80}O_4$ (CNLFO20) ferrites. In addition, the magnetic phase of transition of prepared spinel ferrites CNLFO was explored through online ultrasonic velocity measurement at elevated temperature.

2. Materials and Methods

Ferrites with the general formula $Co_{0.50}Ni_{0.50}La_xFe_{2-x}O_4$ ($0.00 \leqslant x \leqslant 0.2$; step 0.05) were prepared using a sonochemical reactor. Analytical grade metal nitrates cobalt (II) nitrate hexahydrate ($Co(NO_3)_2.6\ H_2O$), nickel(II) nitrate hexahydrate ($Ni(NO_3)_2.6\ H_2O$), ferric nitrate nonahydrate ($Fe(NO_3)_3.9\ H_2O$), lanthanum (III) nitrate ($La(NO_3)_3.6\ H_2O$) and dehydrated citric acid ($C_6H_8O_7$) were used as starting materials. The required stoichiometric quantities of metal nitrates and citric acid weighted using a digital balance were separately dissolved in most minor amounts of doubly distilled water. An earlier work [11,14] has already elaborated on the detailed approach used to obtain $Co_{0.50}Ni_{0.50}La_xFe_{2-x}O_4$ powders. To ensure complete combustion with no NO^{3-} ion filtrates/leftovers, the citric at whole-metal nitrates molar ratio was set to 1:1 [11]. A uniform homogeneous solution was prepared by mixing metal nitrates and citric acid, which was then subjected to sonication for 2 h while maintaining a constant temperature of 80 °C. Following sonication, a 1 M solution of ammonium hydroxide (NH_4OH) was slowly added drop by drop to the mixed solution to adjust the pH to 7.0 at room temperature. At this point, the solution became darker and thicker. The pH-adjusted solution was then heated gradually (to 80 °C) and left in a hot-air oven for 24 h to remove/evaporate the water content. Subsequently, the gel underwent further processing in a muffle furnace at 450 °C for 4 h to eliminate nitrogen oxides. The resulting calcined powder was then carefully ground using an agate mortar until it achieved a fine consistency. This fine powder underwent sintering at 1000 °C in ambient air for 24 h, after which it was cooled down to room temperature in a furnace.

X-ray powder diffraction (XRD) patterns of CNLFO00, CNLFO05, CNLFO10, CNLFO15, and CNLFO20 ferrite samples were collected on a Bruker D8 axis diffractometer with a goniometer using Cu-Kα radiation ($\lambda = 0.15406$ nm) source. The step-scan mode was used to collect/gather the diffracted intensities in an angular range of 10–80°. The crystal structure was refined by applying the Rietveld profile method. The particle size and surface morphology of CNLFO00, CNLFO05, CNLFO10, CNLFO15, and CNLFO20 ferrite samples were explored using the images obtained from the FEI Nova Nano SEM 600 (the Netherlands) field emission scanning electron microscopy (FE-SEM). Room-temperature magnetizations and the temperature-dependent molar magnetic susceptibility of the $Co_{0.50}Ni_{0.50}La_xFe_{2-x}O_4$ samples were measured using a Lakeshore 7410 model vibrating sample magnetometer (VSM). The complex impedance technique measured room temperature dielectric properties as the function of applied frequency. This measurement was conducted employing the PM5 Agilent (USA; B1500A) device analyzer, which utilizes a pulsed source within the frequency range of 0.5 to 3 GHz. The longitudinal ultrasonic velocity ($U_L(T)$) was produced/generated and received using a high-power Olympus (USA) pulse receiver (5900 PR) and X-cut 5 MHz transducers. The ultrasonic waves were digitally recorded using a Wave Runner (104Mxi, 1 GHz) LeCroy (USA) computer-based oscilloscope. An experimental set-up designed in-house was employed to measure the U_L (T) across a temperature range spanning from 300 to 900 K [11].

3. Results and Discussion

XRD patterns of CNLFO00, CNLFO05, CNLFO10, CNLFO15, and CNLFO20 ferrite samples are shown in Fig. 1. The observed (111), (220), (311), (222), (400), (422), (511), and (440) diffraction peaks can be indexed with Fd3m space group of a single phase cubic spinel crystal structure [29,38–40]. The average crystalline size (D_{XRD}), lattice parameters (a), and volume (V) of the unit cell were calculated from XRD patterns using the standard formulas. The average crystalline size (D) of the $Co_{0.50}Ni_{0.50}La_xFe_{2-x}O_4$ ferrite samples was calculated using Scherrer's formula [14]. The obtained values are listed in Table 1 for easy comparison. Table 1 shows that that with increasing La^{3+} content, the crystallite size decreases slightly from 64 nm (for CNLFO00 ferrite) to

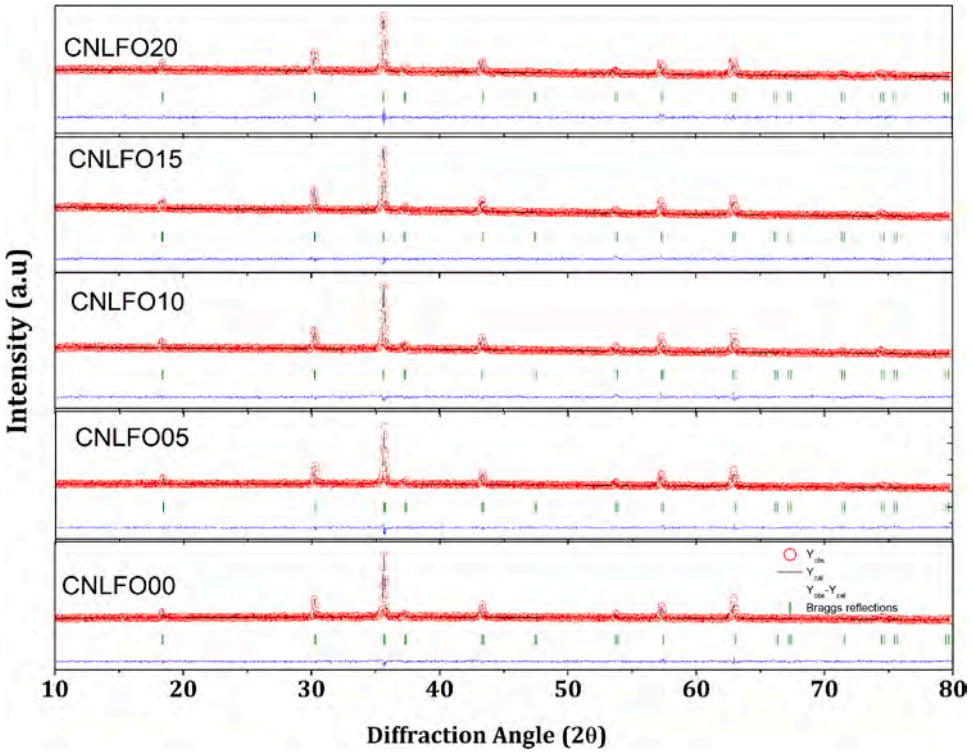

Fig. 1. Refined XRD pattern of the CNLFO00, CNLFO05, CNLFO10, CNLFO15, and CNLFO20 ferrite samples.

Table 1
Average crystallite size, Lattice parameters, Curie temperature (T_C) and magnetic data of CNLFO00, CNLFO05, CNLFO10, CNLFO15, and CNLFO20 ferrite samples.

Parameters	CNLFO00	CNLFO05	CNLFO10	CNLFO15	CNLFO20
Average Crystallite Size (nm)	64	56	47	42	33
Lattice constant (Å)	8.3467	8.3489	8.3498	8.3536	8.3537
Volume of the Unit cell (Å^3)	581.493	581.953	582.141	582.936	582.957
Particle size (nm)	81	46	37	23	20
Curie temperature T_C (K)					
χ_M(T) measurement (T_B)	858.99	842.26	814.90	791.01	761.26
U_L(T) measurement (T_C)	858	843	816	795	762
~ Difference	0.99	0.74	1.10	3.99	0.74
Magnetic parameters					
Saturation magnetization M_s (emu g^{-1})	64.92	60.05	56.49	52.36	48.21
Remnant magnetization M_r (emu g^{-1})	18.62	18.13	14.55	14.48	14.35
M_r/M_s	0.287	0.302	0.258	0.277	0.298
Coercivity H_c (Oe)	315	325	342	356	420

33 nm (for CNLFO20 ferrite). The replacement of Fe^{3+} ions by La^{3+} ions altered the crystallite size and affected the distribution of Fe^{3+}/La^{3+} ions along Co^{2+} and Ni^{2+} sites. It is well known that the size of the crystallite and distribution of $Fe^{3+}/La^{3+}/Co^{2+}/Ni^{2+}$ sites obviously affect the potential customization and modify the electric and magnetic properties of ferrites. This decrease in the grain size observed in $Co_{0.50}Ni_{0.50}La_xFe_{2-x}O_4$ ferrite samples affects the electric/magnetic properties. Thus, the distribution of cations and size of the crystallite play a vital role in controlling/tailoring the electric and magnetic properties of ferrites [41–43]. In addition, the electronic properties of complex ferrite compounds are intricately linked to the average crystallite size and distribution, with a more pronounced influence observed in mezzo- and nano-scale crystallites featuring a diverse distribution spectrum. As crystallite size diminishes, quantum confinement effects become notable, causing alterations in the electronic band structure and resulting in discrete energy levels. In the realm of nano-scale crystallites, these effects manifest as quantized electronic states, thereby modifying the overall electronic properties [44].

Table 1 shows that the lattice constant increases from 8.3467 Å for CNLFO00 ferrite to 8.3537 Å for CNLFO20 ferrite. The lattice parameter and volume of the unit cell increase with increasing La^{3+} substitution. On the other hand, the particle size and average crystalline size decrease with increasing La^{3+} substitution/doping. FE-SEM micrograph of the synthesized CNLFO00, CNLFO05, CNLFO10, CNLFO15, and CNLFO20 ferrite samples is shown in Fig. 2. The average particle size of spherical—like $Co_{0.50}Ni_{0.50}La_xFe_{2-x}O_4$ spinel ferrite samples is shown in Table 1. The particle size of $Co_{0.50}Ni_{0.50}La_xFe_{2-x}O_4$ spinel ferrite samples seems to reduce with increasing La^{3+} ion concentration. This decrease in crystalline and particle size can be clarified when considering substituting the larger ionic radius (La^{3+}, 1.016 Å) instead of Fe^{3+} ions (0.645 Å) and Vegard's law. This ion substitution introduces lattice strain, leading to a reduction in both crystalline and particle size as the lattice structure undergoes modifications to accommodate the larger ionic radius of La^{3+}. Similar reports were available in the literature [45, 46].

Fig. 3 shows the room temperature variation of the dielectric

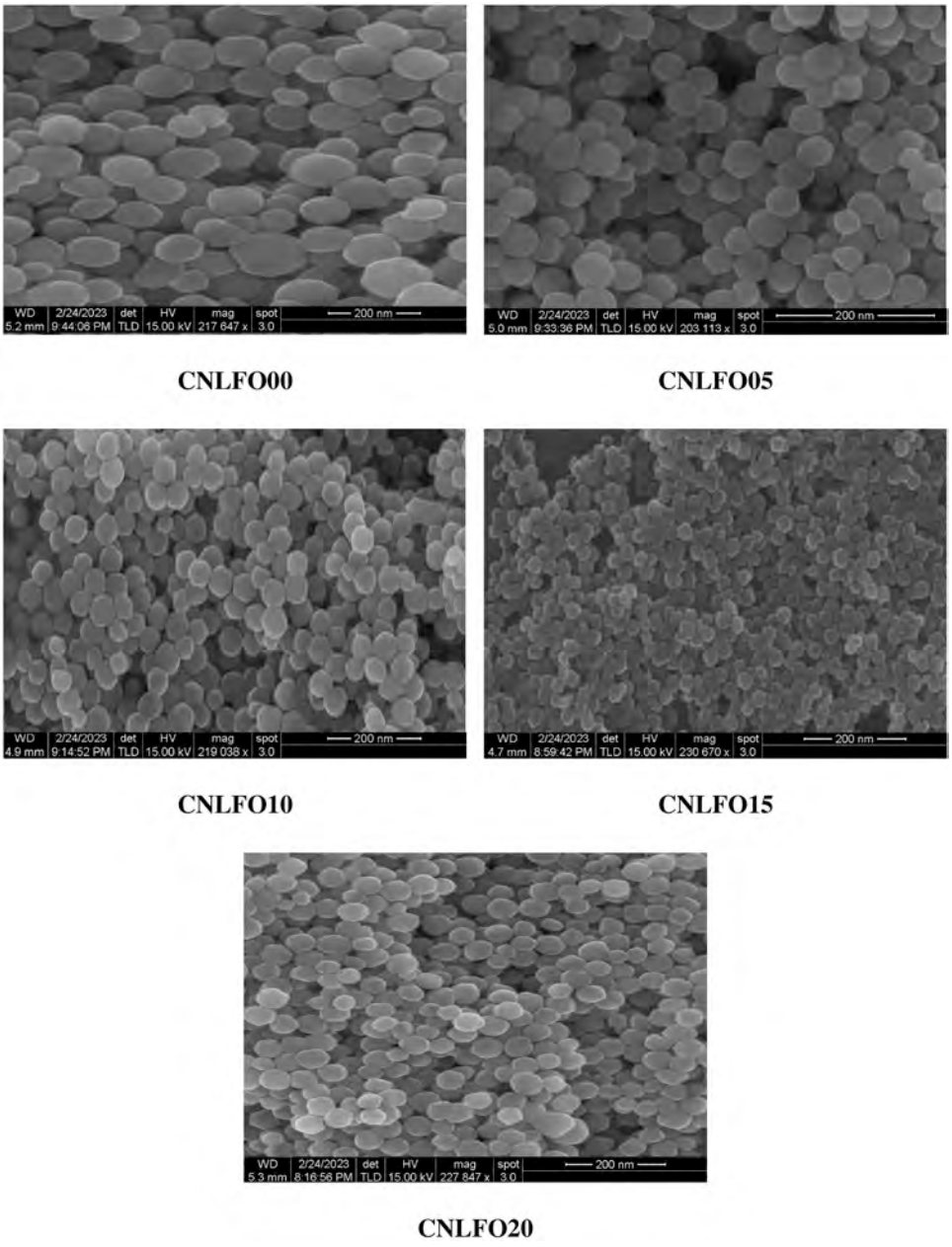

Fig. 2. FE-SEM images of the CNLFO00, CNLFO05, CNLFO10, CNLFO15, and CNLFO20 ferrite samples.

constant (ε′) as a function of the frequency of $Co_{0.50}Ni_{0.50}La_xFe_{2-x}O_4$ spinel ferrite samples. The normal dielectric spreading/dispersion performance was noticed in all CNLFO00, CNLFO05, CNLFO10, CNLFO15, and CNLFO20 ferrite samples. With increasing frequency, the ε′ of CNLFO00, CNLFO05, CNLFO10, CNLFO15, and CNLFO20 ferrite samples decreases. However, ε′ shows a constant behaviour at higher frequencies. The reduction of ε′ at low frequencies range can be attributed to the relaxation polarization and deformational mechanisms [47,48]. The relaxation polarisation is influenced by orientational or interfacial effects, however, the deformational polarisation is dependent on the displacement of electrons and $Fe^{3+}/La^{3+}/Co^{2+}/Ni^{2+}$ ions. The presence of divalent $Co^{2+}/Ni^{2+}/Fe^{2+}$ ions and trivalent Fe^{3+}/La^{3+} ions at octahedral sites states ferrites as the polar nature of materials. The orientational polarisation is caused by the rotational displacements of dipoles. The exchange of electrons between the ions, which causes the dipoles to rotate or turn, can be described by the alignment of the dipoles themselves with the field. Since molecular dipoles require time to alter their alignment in reaction to the applied field, a rise in frequency results in a decrease in orientational polarisation. Therefore, the sudden fall in ε′ is observed with increasing frequency [49].

At room temperature, the study of the dielectric loss tangent (tan δ) as a function of frequency is shown in Fig. 4. Similarly, the increase in frequency has a decreasing effect on the dielectric loss tangent. The Maxwell-Wagner interfacial type polarisation causes dispersion in CNLFO00, CNLFO05, CNLFO10, CNLFO15, and CNLFO20 ferrite samples [48–50]. The numeral of influences such as ionic composition, stoichiometry, nature atoms in tetrahedral/octahedral exchange, calcination/sintering temperature, and structural homogeneity of the samples on dielectric loss tangent. However, Fig. 3 and Fig. 4 indicate that dielectric constant and dielectric loss of CNLFO00, CNLFO05, CNLFO10, CNLFO15, and CNLFO20 ferrite samples depend upon the composition; both ε′ and tan δ increase as the amount of La^{3+} increases. The La^{3+} substituted $Co_{0.50}Ni_{0.50}La_xFe_{2-x}O_4$ spinel ferrite samples have shown high ε′ compared to the pure $Co_{0.50}Ni_{0.50}Fe_2O_4$ (CNLFO00) spinel ferrite samples ferrite. Due to the incorporation of La^{3+} in CNLFO00, a clear dispersion in ε′ has been observed in the lower frequency region which is

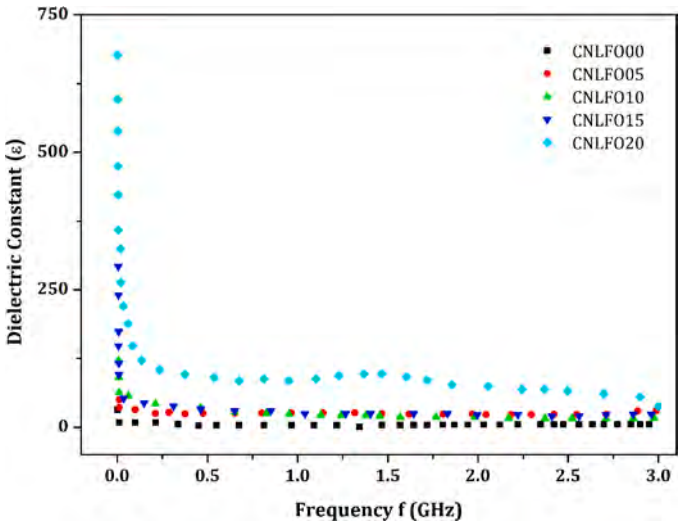

Fig. 3. Real-part dielectric constant of the CNLFO00, CNLFO05, CNLFO10, CNLFO15, and CNLFO20 ferrite samples.

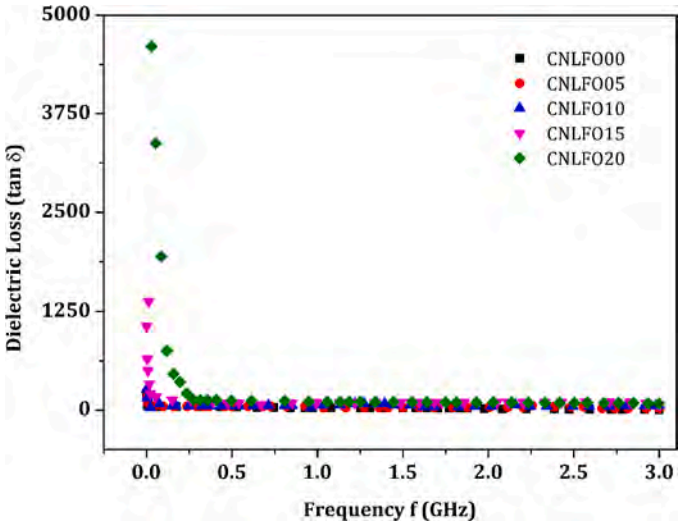

Fig. 4. Dielectric loss of the CNLFO00, CNLFO05, CNLFO10, CNLFO15, and CNLFO20 ferrite samples.

attributed to interfacial polarization [48,49]. This La^{3+} substitution also led to a decrease in grain size (Table 1) and an increase in the specific surface area of the particle. The dielectric constant of CNLFO00, CNLFO05, CNLFO10, CNLFO15, and CNLFO20 ferrite samples at low frequencies rises as a result of space charge polarization, which significantly subsidizes the high value of ε′ of the material, as grain boundaries have broadened and become more active at low frequencies. The value ε' of doped spinel ferrites increased as a result of high radius La^{3+} substitution can also be related to distortion/alternation of the lattice and an increase in the length of the La^{3+}-O^{2-} bond at octahedral sites, which upshots in an intensification in atomic polarizability [51,52].

The trace variation of the magnetization M as a function of the applied magnetic fields H for various CNLFO00, CNLFO05, CNLFO10, CNLFO15, and CNLFO20 ferrite samples were measured at room temperature. The magnetic hysteresis curves of $Co_{0.50}Ni_{0.50}La_xFe_{2-x}O_4$ spinel ferrite samples are shown in Fig. 5. These curves were used to obtain the magnetic parameters such as saturation magnetization (M_S), remanent magnetization (M_r), and the coercive field (H_C). The obtained values are listed in Table 1. The M_S, and M_r showed a decrease monotonically with the content of La^{3+}. The pristine CNLFO00, ferrite sample,

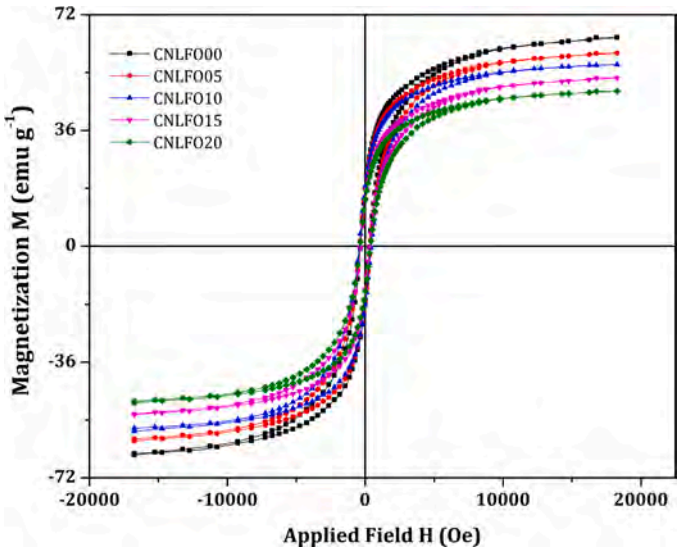

Fig. 5. Room temperature hysteresis loop of the CNLFO00, CNLFO05, CNLFO10, CNLFO15, and CNLFO20 ferrite samples.

and La^{3+} co-substituted CNLFO05, CNLFO10, CNLFO15, and CNLFO20 ferrite samples have shown decreased M_S and M_R and increased H_C values. The squareness ratio value of La^{3+} doped $Co_{0.50}Ni_{0.50}La_xFe_{2-x}O_4$ ferrite samples less than 0.5 indicates that the prepared $Co_{0.50}Ni_{0.50}La_xFe_{2-x}O_4$ samples have a lower remnant magnetization relative to its saturation magnetization. A squareness ratio below 0.5 suggests that CNLF00, CNLFO05, CNLFO10, CNLFO15, and CNLFO20 ferrite samples do not retain as much magnetization when the external magnetic field is removed compared to their maximum magnetization capacity. These La^{3+} doped $Co_{0.50}Ni_{0.50}La_xFe_{2-x}O_4$ ferrite samples might be more suitable for applications where a quick response to changes in magnetic fields is needed, as they can switch between magnetic states more easily due to their lower remnant magnetization [53,54].

The net magnetic moment of spinel systems is the difference between the magnetic moments of B-site and A-site. Subsequently, the exchange of Fe^{3+} (magnetic ions) by La^{3+} (non-magnetic ions) ions reduces the net magnetization for the CNLFO samples, in worthy arrangement with the previous studies [55,56]. The doping of La^{3+} ions instead of Fe^{3+} ions leads to occupy the La^{3+} ions in the octahedral site. This octahedral site occupancy of nonmagnetic La^{3+} ions is leading to the decrease of the super-exchange interaction between the A- and B-sites and to reducing/increasing the magnetization of the B-site/A-site and successively the net magnetization of the ferrite system was reduced. Further, the local structural changes are due to cation distribution between the octahedral and tetrahedral positions (B and A- sites; distribution of cations at lattice sites) of the spinel system. The surface effect, magnetocrystalline anisotropy, lattice imperfections, dislocations, homogeneity, porosity, morphology, internal strain density, particle size, and secondary phases the particle size affect the magnetic behavior of these nanoferrites. The determined values of the remanent magnetization ratio for CNLFO00, CNLFO05, CNLFO10, CNLFO15, and CNLFO20 ferrite samples are approximately 18.62, 18.13, 14.55, 14.48, and 14.35, respectively. The remanent magnetization ratio (M_r/M_s) varies slightly from 0.287 for the CNLFO00 sample to 0.298 for the CNLFO20 sample. This result refers to the lesser reduction of the anisotropic behavior within the studied ferrite samples. The high anisotropy model of CNLFO00 ferrite is due to the large concentration of Co^{2+} and Ni^{2+} ions at the octahedral site [57,58].

Further, the variations in oxygen levels can impact the oxidation degree of 3d-metals, altering magnetic and electrical parameters. Changes in oxygen content influence magnetic properties like total magnetic moment and Curie point, as well as electrical features such as

dc- and ac-conductivity and band gap. Additionally, oxygen vacancies influence exchange interactions, with increased vacancy concentration leading to a decrease in interaction intensity. In complex oxides, indirect exchange prevails, and near oxygen vacancies, the exchange is negative according to Goodenough-Kanamori rules, resulting in the formation of a weak magnetic state [59,60]. However, La^{3+} can play a crucial role in controlling the oxidation states of iron ions in ferrites by stabilizing the + 3 oxidation state, modifying the electronic structure, influencing magnetic properties, and controlling crystal defects [61,62]. Furthermore, the magnetic characteristics of ferrites are closely tied to crystallite size. In nano-scale crystallites, unique magnetic features, such as super-paramagnetic behavior, can emerge. Additionally, smaller crystallites may showcase variations in magnetic anisotropy, coercivity, and saturation magnetization [44].

The measured molar magnetic susceptibility (χ_M) as a function of temperature from 300 to 900 K for the CNLFO00, CNLFO05, CNLFO10, CNLFO15, and CNLFO20 ferrite samples is shown in Fig. 6. χ_M(T) as the function of temperature is the best tool to recognize the specific magnetic transition temperatures in the materials. The pattern χ_M (T) is the same for undoped CNLFO00 and doped CNLFO05, CNLFO10, CNLFO15, and CNLFO20 ferrite samples. This χ_M (T) graph shows the ferromagnetic (FM) to paramagnetic nature of the prepared sample during heating. Temperature increases cause a decrease in χ_M(T). As a result, it indicates the decline in ferromagnetism when temperature rises. The paramagnetic zone is eventually reached after the blocking temperature (T_B), where a fully/completely disordered state and magnetization destruction are achieved. At the blocking temperature (T_B), the thermal energy is strong enough to disturb all the aligned spins, causing χ_M (T) to drop dramatically. The T_B values are 858.99, 842.26, 814.90, 791.01, and 761.26 K for CNLFO00, CNLFO05, CNLFO10, CNLFO15, and CNLFO20 ferrite samples respectively. The T_B marked for La^{3+} doped $Co_{0.50}Ni_{0.50}La_xFe_{2-x}O_4$ ferrite samples is listed in Table 1.

Temperature-dependent longitudinal ultrasonic velocity of the CNLFO00, CNLFO05, CNLFO10, CNLFO15, and CNLFO20 ferrite samples obtained as a function of temperature is demonstrated in Fig. 7. The temperature-dependent U_L(T) measurement could be used to explore phase transition and structural transition in materials. The through-transmission approach was used to investigate/measure temperature-dependent U_L(T) of the CNLFO00, CNLFO05, CNLFO10, CNLFO15, and CNLFO20 ferrite samples. The sensitive variation in the lattice arrangement of the ferrite at transition temperature gives to abrupt change in elastic constants of the crystal. Therefore, the observed variation at the transition temperature shows a predominate dip in U_L(T) which represents the scale of the transition temperature. When the temperature increases, the U_L(T) of the materials is monotonically

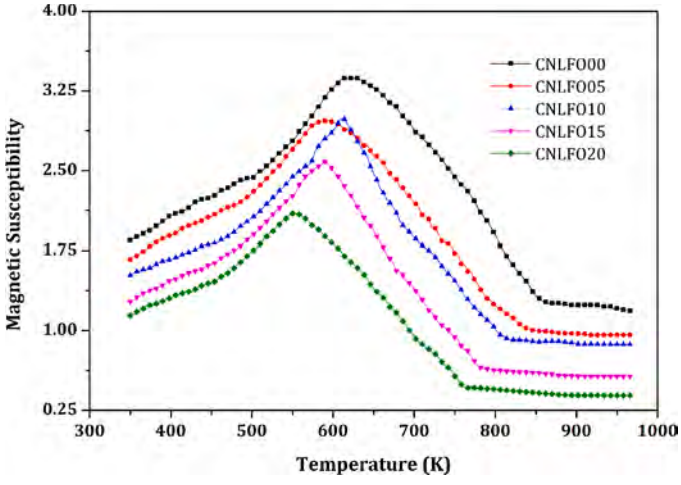

Fig. 6. Temperature dependent magnetic susceptibility of the CNLFO00, CNLFO05, CNLFO10, CNLFO15, and CNLFO20 ferrite samples.

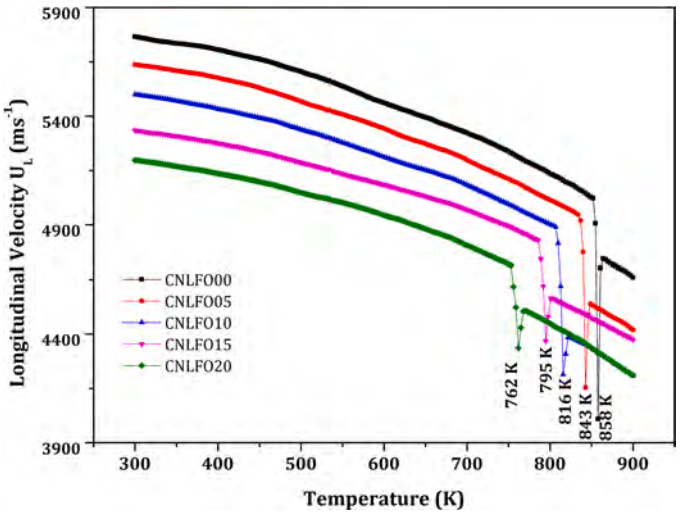

Fig. 7. Temperature dependent ultrasonic velocity of the CNLFO00, CNLFO05, CNLFO10, CNLFO15, and CNLFO20 ferrite samples.

dropped. An abrupt change in the U_L(T) is used to determine the T_C of the sample. The temperature-dependent ultrasonic measurements can detect subtle changes in material properties, including alterations in elastic properties, which can relate to phase transitions (T_C). The variations in the speed of sound or attenuation can indicate phase transitions, including the shift from ferromagnetism to paramagnetism at the T_C. The anomaly temperature marked from temperature-dependent U_L(T) is given in Table 1. The determined T_C for CNLFO00, CNLFO05, CNLFO10, CNLFO15, and CNLFO20 ferrite samples are 858, 843, 816, 795, and 762 K respectively. The T_C of the sample represents the domain rotation and thermal stability of a spin alignment. The reduction of superexchange interactions between the magnetic moments and spins that existed in the ferrites leads to a lowering of the T_C [10] and to an abrupt alteration/transformation in the lattice of the ferrite. At octahedral sites, the Fe–Fe interaction is much stronger than the Fe–La interaction [63,64]. The doping of nonmagnetic La^{3+} ions at octahedral sites causes a decline in the Curie temperature due to the change in interaction angles between Fe^{3+}- O- Fe^{3+} and Fe^{3+}- Fe^{3+} [65–68].

The T_B noted from temperature-dependent molar magnetic susceptibility (χ_M(T)) for the CNLFO00, CNLFO05, CNLFO10, CNLFO15, and CNLFO20 ferrite samples is compared with the T_C noted from temperature-dependent U_L(T) derived from the measured transition time [69,70]. The small difference in T_C has existed. In this study, T_C measured from ultrasonic measurement depends on the blocking temperature (T_B). The variation in T_C and T_B was used to explain the orientation of the domain walls. The blocking temperature influences the susceptibility measurement (T_B) through the domain wall movement. The direction of the domain walls was explained in terms of the variance in T_C and T_B. Thermal excitations at temperature T_B cause the magnetic moments of various particles to be randomly orientated. The T_B temperature relates to the freezing of magnetic moments in small particles due to thermal energy, while the transition temperature, often represented by the T_C, denotes the point at which the ferrite material transitions from a ferromagnetic to a paramagnetic state. Both temperatures are crucial in understanding the magnetic behavior of materials like ferrites under different thermal conditions.

Furthermore, according to scientific data for diverse samples, the variation difference in T_B and T_C was greater than 60 K [71,72]. The difference between T_B and T_C in the current study is quite small (4 K). The thermal energy at T_C causes randomization of the spins within various particles; generally, T_B is less than T_C, which coincides well with the current experiment. The difference between the results of the susceptibility measurement and ultrasonic longitudinal measurements of the La^{3+} ion-doped CNLFO00, CNLFO05, CNLFO10, CNLFO15, and

CNLFO20 ferrite samples suggests that the ultrasonic NDT measurement is a flexible method for determining the phase transition temperature of spinel ferrites. The noticeable reduction in the transition temperature and average particle size observed in the doped CNLFO05, CNLFO10, CNLFO15, and CNLFO20 ferrite samples, as compared to the undoped CNLFO00 sample, can be ascribed to the elevated binding energy associated with the rare earth ions' La^{3+}-O^{2-} bond, contrasting with the Fe^{3+}-O^{2-} bond. The higher binding energy essentially acts as a hindrance to the growth of grains within the material. As a result, even with an increase in the doping concentration, this effect persists as anticipated. The lowering the transition temperature (T_C) of ferrite samples offers advantages, enhancing magnetic properties like susceptibility and saturation magnetization. This improvement is valuable in applications like magnetic recording, sensors, and biomedical uses, particularly in hyperthermia treatments. The CNLFO00, CNLFO05, CNLFO10, CNLFO15, and CNLFO20 ferrite samples have T_C (above room temperature) and microstructural (magnetic and electrical results) values are very helpful for harvesting multilayer chip inductors.

4. Conclusion

The La^{3+} substituted $Co_{0.50}Ni_{0.50}La_xFe_{2-x}O_4$ ferrite samples were successfully synthesized by the sonochemical method and the XRD spinel ferrite pattern was demonstrated. In comparison to pure $Co_{0.50}Ni_{0.50}Fe_2O_4$ spinel ferrite sample, the La^{3+} substituted $Co_{0.50}Ni_{0.50}La_xFe_{2-x}O_4$ spinel ferrite samples had a higher dielectric constant. A clear dispersion in the dielectric constant has been observed in the lower frequency region due to the incorporation of La^{3+} ions. Due to the diminished superexchange interactions between Fe^{3+}-Fe^{3+} ions and the octahedral positions, it was discovered that the saturation magnetization decreased in La^{3+} ion-doped ferrites. The temperature-dependent in-situ ultrasonic NDT and susceptibility measurements were used to determine the transition temperature values for the La^{3+} substituted $Co_{0.50}Ni_{0.50}La_xFe_{2-x}O_4$ ferrite samples. The difference between the blocking temperature and Curie temperature in the current study is quite small (4 K). This observed difference implies that finding the phase transition temperature of spinel ferrites using ultrasonic NDT testing is a flexible process.

CRediT authorship contribution statement

Sivakumar R.: Writing – original draft, Validation, Resources. **Rajkumar G.:** Writing – review & editing, Writing – original draft, Visualization, Validation, Conceptualization. **Ganesh Babu B.:** Writing – review & editing, Resources, Project administration, Data curation. **K SAKTHIPANDI:** Writing – review & editing, Writing – original draft, Validation, Supervision, Methodology, Investigation, Formal analysis, Data curation, Conceptualization. **Venkatesan K.:** Investigation, Formal analysis, Data curation. **Arunmetha S.:** Writing – review & editing, Visualization, Software, Resources, Data curation. **Hossain Aslam:** Writing – review & editing, Writing – original draft, Visualization, Validation, Resources, Project administration. **Raghavan M.:** Writing – review & editing, Resources, Investigation, Formal analysis. **Rajendran V.:** Writing – review & editing, Visualization.

Declaration of Competing Interest

None.

The authors declare that they have no known competing financial interests or personal relationships that could have appeared to influence the work reported in this paper.

Data Availability

Data will be made available on request.

Acknowledgement

A.H. acknowledges the financial support from the Strategic Academic Leadership Program of the Southern Federal University ("Priority 2030").

References

[1] D.A. Vinnik, D.P. Sherstyuk, V.E. Zhivulin, D.E. Zhivulin, A.Y. Starikov, S. A. Gudkova, D.A. Zherebtsov, D.A. Pankratov, Y.A. Alekhina, N.S. Perov, S. V. Trukhanov, E.L. Trukhanova, A.V. Trukhanov, Impact of the Zn–Co content on structural and magnetic characteristics of the Ni spinel ferrites, Ceram. Int. 48 (2022) 18124–18133, https://doi.org/10.1016/j.ceramint.2022.03.070.

[2] M. Kamran, M. Anis-ur-Rehman, Study of dielectric and electrical properties in Co-(Fe–Ce-Nd) nanosized spinel ferrites, Mater. Sci. Semicond. Process. 153 (2023) 107111, https://doi.org/10.1016/j.mssp.2022.107111.

[3] S. Singhal, R. Sharma, T. Namgyal, S. Jauhar, S. Bhukal, J. Kaur, Structural, electrical and magnetic properties of $Co_{0.5}Zn_{0.5}Al_xFe_{2-x}O_4$ (x= 0, 0.2, 0.4, 0.6, 0.8 and 1.0) prepared via sol–gel route, Ceram. Int. 38 (2012) 2773–2778, https://doi.org/10.1016/j.ceramint.2011.11.047.

[4] D.B. Migas, V.A. Turchenko, A.V. Rutkauskas, S.V. Trukhanov, T.I. Zubar, D. I. Tishkevich, A.V. Trukhanov, N.V. Skorodumova, Temperature induced structural and polarization features in $BaFe_{12}O_{19}$, J. Mater. Chem. C. 11 (2023) 12406–12414, https://doi.org/10.1039/D3TC01533E.

[5] R. Shunmuga Priya, P. Chaudhary, E. Ranjith Kumar, A. Balamurugan, C. Srinivas, G. Prasad, M. Deepty, V. Praveenkumar, B.C. Yadav, D.L. Sastry, Y. Al-Douri, Effect of heat treatment on structural, morphological, dielectric and magnetic properties of Mg–Zn ferrite nanoparticles, Ceram. Int. 48 (2022) 15243–15251, https://doi.org/10.1016/j.ceramint.2022.02.056.

[6] B. Jiang, W. Yang, H. Bai, C. Wang, C. Xu, Z. Li, L. Yan, C. Zhang, N. Wu, S. Che, X. Wang, Y. Li, Facile fabrication of Fe/Fe_5C_2@N-doped porous carbon as an efficient microwave absorbent with strong and broadband absorption properties at an ultralow filler loading, Carbon 196 (2022) 890–901, https://doi.org/10.1016/j.carbon.2022.05.045.

[7] T. Dippong, E.A. Levei, O. Cadar, Investigation of structural, morphological and magnetic properties of MFe_2O_4 (M = Co, Ni, Zn, Cu, Mn) obtained by thermal decomposition, Int. J. Mol. Sci. 23 (2022) 8483, https://doi.org/10.3390/ijms23158483.

[8] A. Mahmood, A. Maqsood, Physical characterization, optical properties, and magnetic interactions of cadmium-doped zinc ferrite nanoparticles, J. Supercond. Nov. Magn. 35 (2022) 3379–3395, https://doi.org/10.1007/s10948-022-06367-6.

[9] A. Manthiram, John Goodenough's 100th birthday celebration: his impact on science and humanity, ACS Energy Lett. 7 (2022) 2404–2406, https://doi.org/10.1021/acsenergylett.2c01343.

[10] S. Aman, M.B. Tahir, N. Ahmad, Study of Europium substituted spinel ferrites for microwave devices, J. Mater. Sci. Mater. Electron. 33 (2022) 21995–22006, https://doi.org/10.1007/s10854-022-08990-4.

[11] K. Sakthipandi, B. Ganesh Babu, G. Rajkumar, A. Hossian, M. Srinidhi Raghavan, M. Rajesh Kumar, Investigation of magnetic phase transitions in $Ni_{0.5}Cu_{0.25}Zn_{0.25}Fe_{2-x}La_x\ O_4$ nanoferrites using magnetic and in-situ ultrasonic measurements, Phys. B Condens. Matter 645 (2022) 414280, https://doi.org/10.1016/j.physb.2022.414280.

[12] M.B. Mohamed, K. EL-Sayed, Structural, magnetic and dielectric properties of (PANI)–Ni0.5Zn0.5Fe1.5Cr0.5O4 nanocomposite, Compos. Part B Eng. 56 (2014) 270–278, https://doi.org/10.1016/j.compositesb.2013.08.038.

[13] Z.K. Heiba, A. Abo-Shama, M. Bakr, K. El-Sayed, Effect of partial substitution of Cr or Mn for Ga or Fe on crystal-structure and microstructures of $GaFeO_3$, Powder Diffr. 22 (2007) 256–258, https://doi.org/10.1154/1.2770471.

[14] N. Lenin, K. Sakthipandi, R. Rajesh Kanna, G. Rajkumar, Electrical, magnetic and structural properties of polymer-blended lanthanum-added nickel nano-ferrites, Ceram. Int. 44 (2018) 21866–21873, https://doi.org/10.1016/j.ceramint.2018.08.295.

[15] Q. Zhao, Z. Yan, C. Chen, J. Chen, Spinels: controlled preparation, oxygen reduction/evolution reaction application, and beyond, Chem. Rev. 117 (2017) 10121–10211, https://doi.org/10.1021/acs.chemrev.7b00051.

[16] S.B. Narang, K. Pubby, Nickel spinel ferrites: a review, J. Magn. Magn. Mater. 519 (2021) 167163, https://doi.org/10.1016/j.jmmm.2020.167163.

[17] A. Hao, X. Ning, Recent advances in spinel ferrite-based thin films: synthesis, performances, applications, and beyond, Front. Mater. 8 (2021), https://doi.org/10.3389/fmats.2021.718869.

[18] D.S. Mathew, R.-S. Juang, An overview of the structure and magnetism of spinel ferrite nanoparticles and their synthesis in microemulsions, Chem. Eng. J. 129 (2007) 51–65, https://doi.org/10.1016/j.cej.2006.11.001.

[19] A. Soufi, H. Hajjaoui, R. Elmoubarki, M. Abdennouri, S. Qourzal, N. Barka, Spinel ferrites nanoparticles: synthesis methods and application in heterogeneous fenton oxidation of organic pollutants – a review, Appl. Surf. Sci. Adv. 6 (2021) 100145, https://doi.org/10.1016/j.apsadv.2021.100145.

[20] J. Jing, L. Liangchao, X. Feng, Structural analysis and magnetic properties of Gd-doped Li-Ni ferrites prepared using rheological phase reaction method, J. Rare Earths. 25 (2007) 79–83, https://doi.org/10.1016/S1002-0721(07)60049-0.

[21] B.L. Shinde, U.M. Mandle, A.M. Pachpinde, K.S. Lohar, Synthesis and characterization of Al3+ substituted Ni–Cu–Zn nano ferrites, J. Therm. Anal. Calorim. 147 (2022) 2947–2956, https://doi.org/10.1007/s10973-021-10719-0.

[22] X. Xie, B. Wang, Y. Wang, C. Ni, X. Sun, W. Du, Spinel structured MFe_2O_4 (M = Fe, Co, Ni, Mn, Zn) and their composites for microwave absorption: A review, Chem. Eng. J. 428 (2022) 131160, https://doi.org/10.1016/j.cej.2021.131160.

[23] C. Srinivas, K. Naga Praveen, E. Ranjith Kumar, S. Singh, S. Singh Meena, P. Bhatt, T.V. Chandrasekhar Rao, D. Sarkar, B. Arun, K.C. James Raju, D.L. Sastry, Microwave absorption properties of rare earth (RE) ions doped Mn–Ni–Zn nanoferrites (RE = Dy, Sm, Ce, Er) to shield electromagnetic interference (EMI) in X-band frequency, Ceram. Int. 48 (2022) 33891–33900, https://doi.org/10.1016/j.ceramint.2022.07.338.

[24] M. Maisnam, Magnetic hysteresis properties of sol-gel synthesized Li-Co-Y ferrites, Ferroelectrics 587 (2022) 56–62, https://doi.org/10.1080/00150193.2022.2034414.

[25] S. Ajia, H. Asa, Y. Toyoda, M. Sato, M. Matsuura, N. Tezuka, S. Sugimoto, Development of an alternative approach for electromagnetic wave absorbers using Fe–Cr–Co alloy powders, J. Alloy. Compd. 903 (2022) 163920, https://doi.org/10.1016/j.jallcom.2022.163920.

[26] I.H. Gul, A.Z. Abbasi, F. Amin, M. Anis-ur-Rehman, A. Maqsood, Structural, magnetic and electrical properties of $Co_{1-x}Zn_xFe_2O_4$ synthesized by co-precipitation method, J. Magn. Magn. Mater. 311 (2007) 494–499, https://doi.org/10.1016/j.jmmm.2006.08.005.

[27] M. Shakil, U. Inayat, N.R. Khalid, M. Tanveer, S.S.A. Gillani, N.H. Tariq, A. Shah, A. Mahmood, A. Dahshan, Enhanced structural, optical, and photocatalytic activities of Cd–Co doped Zn ferrites for degrading methyl orange dye under irradiation by visible light, J. Phys. Chem. Solids 161 (2022) 110419, https://doi.org/10.1016/j.jpcs.2021.110419.

[28] M.A. Darwish, M.M. Hussein, S.A. Saafan, W. Abd-Elaziem, D. Zhou, M.V. Silibin, S.V. Trukhanov, N.V. Abmiotka, M.I. Sayyed, D.I. Tishkevich, A.V. Trukhanov, Impact of the Mg/Zn ratio on features of structural and magnetic properties in A-site stoichiometric nanosized spinel ferrites, J. Alloy. Compd. 968 (2023) 172278, https://doi.org/10.1016/j.jallcom.2023.172278.

[29] S.R. Gibin, P. Sivagurunathan, Synthesis and characterization of nickel cobalt ferrite ($Ni_{1-x}Co_xFe_2O_4$) nano particles by co-precipitation method with citrate as chelating agent, J. Mater. Sci. Mater. Electron. 28 (2017) 1985–1996, https://doi.org/10.1007/s10854-016-5755-z.

[30] M. Abdellatif-Youssef, M. Etter, P. Fromme, M. Salerno, Extended properties of magnetic spins of zinc ferrite nanoparticles in the THz frequency range, J. Magn. Magn. Mater. 525 (2021) 167574, https://doi.org/10.1016/j.jmmm.2020.167574.

[31] N.B. Velhal, N.D. Patil, A.R. Shelke, N.G. Deshpande, V.R. Puri, Structural, dielectric and magnetic properties of nickel substituted cobalt ferrite nanoparticles: Effect of nickel concentration, AIP Adv. 5 (2015), https://doi.org/10.1063/1.4931908.

[32] J. Hu, Y. Ma, X. Kan, C. Liu, X. Zhang, R. Rao, M. Wang, G. Zheng, Investigations of Co substitution on the structural and magnetic properties of Ni-Zn spinel ferrite, J. Magn. Magn. Mater. 513 (2020) 167200, https://doi.org/10.1016/j.jmmm.2020.167200.

[33] R.E. El-Shater, H. El Shimy, S.A. Saafan, M.A. Darwish, D. Zhou, K.C.B. Naidu, M. U. Khandaker, Z. Mahmoud, A.V. Trukhanov, S.V. Trukhanov, F. Fakhry, Fabrication of doped ferrites and exploration of its structure and magnetic behavior, Mater. Adv. 4 (2023) 2794–2810, https://doi.org/10.1039/d3ma00105a.

[34] M.A. Almessiere, S. Güner, Y. Slimani, M. Hassan, A. Baykal, M.A. Gondal, U. Baig, S.V. Trukhanov, A.V. Trukhanov, Structural and magnetic properties of $Co_{0.5}Ni_{0.5}Ga_{0.01}Gd_{0.01}Fe_{1.98}O_4/ZnFe_2O_4$ spinel ferrite nanocomposites: Comparative study between sol-gel and pulsed laser ablation in liquid approaches, Nanomaterials 11 (2021) 2461, https://doi.org/10.3390/nano11092461.

[35] M.A. Almessiere, N.A. Algarou, Y. Slimani, A. Sadaqat, A. Baykal, A. Manikandan, S.V. Trukhanov, A.V. Trukhanov, I. Ercan, Investigation of exchange coupling and microwave properties of hard/soft $(SrNi_{0.02}Zr_{0.01}Fe_{11.96}O_{19})/(CoFe_2O_4)_x$ nanocomposites, Mater. Today Nano 18 (2022) 100186, https://doi.org/10.1016/j.mtnano.2022.100186.

[36] A.V. Trukhanov, M.A. Almessiere, A. Baykal, Y. Slimani, E.L. Trukhanova, A. V. Timofeev, V.G. Kostishin, S.V. Trukhanov, M. Sertkol, A. Ul-Hamid, Correlation between the composition, structural parameters and magnetic properties of spinel-based functional nanocomposites, Nano-Struct. Nano-Objects 33 (2023) 100941, https://doi.org/10.1016/j.nanoso.2023.100941.

[37] E. Ahilandeswari, K. Sakthipandi, R. Rajesh Kanna, G. Rajkumar, B. Ganesh Babu, S. Arunmetha, Aslam Hossain, P. Sakthivel, V. Rajendran, M.Srinidhi Raghavan, Exploring the electromagnetic shielding behavior of lanthanum doped calcium nanoferrites (Article in Press), J. Rare Earths (2023), https://doi.org/10.1016/j.jre.2023.11.002.

[38] N. Jahan, M.N.I. Khan, M.R. Hasan, M.S. Bashar, A. Islam, M.K. Alam, M.A. Hakim, J.I. Khandaker, Correlation among the structural, electric and magnetic properties of Al^{3+} substituted Ni–Zn–Co ferrites, RSC Adv. 12 (2022) 15167–15179, https://doi.org/10.1039/D1RA09354A.

[39] P.N. Dave, R. Sirach, M.P. Deshpande, Evaluating the effect of nanosized $CoCuFe_2O_4$ for thermal decomposition of nitrotriazolone high energetic material, ChemistrySelect 7 (2022), https://doi.org/10.1002/slct.202202071.

[40] M. Sundararajan, M. Sukumar, C.S. Dash, A. Sutha, S. Suresh, M. Ubaidullah, A. M. Al-Enizi, M.K. Raza, D. Kumar, A comparative study on $NiFe_2O_4$ and $ZnFe_2O_4$ spinel nanoparticles: Structural, surface chemistry, optical, morphology and magnetic studies, Phys. B Condens. Matter 644 (2022) 414232, https://doi.org/10.1016/j.physb.2022.414232.

[41] H. Nikmanesh, E. Jaberolansar, P. Kameli, A.G. Varzaneh, Effect of praseodymium in cation distribution, and temperature-dependent magnetic response of cobalt spinel ferrite nanoparticles, Nanotechnology 33 (2022) 275709, https://doi.org/10.1088/1361-6528/ac5ee4.

[42] R. Shunmuga Priya, P. Chaudhary, E. Ranjith Kumar, A. Balamurugan, C. Srinivas, G. Prasad, M. Deepty, V. Praveenkumar, B.C. Yadav, D.L. Sastry, Y. Al-Douri, Effect of heat treatment on structural, morphological, dielectric and magnetic properties of Mg–Zn ferrite nanoparticles, Ceram. Int. 48 (2022) 15243–15251, https://doi.org/10.1016/j.ceramint.2022.02.056.

[43] S. Nandy, M. Latwal, G. Pandey, K.H. Chae, Synthesis of nanostructured ferrites and cation distribution studies by X-ray magnetic circular dichroism, Mössbauer spectroscopy, and X-ray absorption spectroscopy, J. Electron. Mater. 51 (2022) 6663–6688, https://doi.org/10.1007/s11664-022-09951-7.

[44] S.V. Trukhanov, V.V. Fedotova, A.V. Trukhanov, H. Szymczak, C.E. Botez, Cation ordering and magnetic properties of neodymium-barium manganites, Tech. Phys. 53 (2008) 49–54, https://doi.org/10.1134/S106378420801009X.

[45] J.K. Khan, M. Khalid, G. Mustafa, Z. Uddin, M. Saleem, A.A. Azam, Study of lanthanum ions (La^{3+}) doped Manganese-Cobalt (Mn-Co) based spinel ferrite nanoparticles for technological applications, Appl. Phys. A. 128 (2022) 961, https://doi.org/10.1007/s00339-022-06106-7.

[46] C.S. Kim, S.W. Lee, S.I. Park, J.Y. Park, Y.J. Oh, Atomic migration in Ni–Co ferrite, J. Appl. Phys. 79 (1996) 5428–5430, https://doi.org/10.1063/1.362328.

[47] E.A. Arrasheed, Y.A. Alibwaini, T.M. Meaz, A.-W. Ajlouni, R.M. Shalaby, O. M. Hemeda, A.M.A. Henaish, The influence of aluminum's crystalline structure on the elastic, dielectric, and electrical properties of Ni ferrite, Phys. Scr. 97 (2022) 115701, https://doi.org/10.1088/1402-4896/ac95dd.

[48] S. Yonatan Mulushoa, N. Murali, Comparison of Structural, dielectric and magnetic investigation of Cr^{3+} substituted Mg-Cu, Mg-Zn, and Mg-Ni ferrites system, Inorg. Chem. Commun. 145 (2022) 110033, https://doi.org/10.1016/j.inoche.2022.110033.

[49] E.A. Arrasheed, Y.A. Alibwaini, T.M. Meaz, A.-W. Ajlouni, R.M. Shalaby, O. M. Hemeda, A.M.A. Henaish, The influence of aluminum's crystalline structure on the elastic, dielectric, and electrical properties of Ni ferrite, Phys. Scr. 97 (2022) 115701, https://doi.org/10.1088/1402-4896/ac95dd.

[50] M. Zulqarnain, S.S. Ali, U. Hira, J.F. Feng, M.I. Khan, M. Rizwan, K. Javed, G. Farid, M.S. Hasan, Superparamagnetic contributions, optical band gap tuning and dominant interfacial resistive mechanisms in ferrites nanostructures, J. Alloy. Compd. 894 (2022) 162431, https://doi.org/10.1016/j.jallcom.2021.162431.

[51] M.P. Ghosh, S. Datta, R. Sharma, K. Tanbir, M. Kar, S. Mukherjee, Copper doped nickel ferrite nanoparticles: Jahn-Teller distortion and its effect on microstructural, magnetic and electronic properties, Mater. Sci. Eng. B. 263 (2021) 114864, https://doi.org/10.1016/j.mseb.2020.114864.

[52] Aakash, R. Choubey, D. Das, S. Mukherjee, Effect of doping of manganese ions on the structural and magnetic properties of nickel ferrite, J. Alloy. Compd. 668 (2016) 33–39, https://doi.org/10.1016/j.jallcom.2016.01.198.

[53] S. Prasad, N. Gajbhiye, Magnetic studies of nanosized nickel ferrite particles synthesized by the citrate precursor technique, J. Alloy. Compd. 265 (1998) 87–92, https://doi.org/10.1016/S0925-8388(97)00431-3.

[54] V.K. Chakradhary, A. Ansari, M.J. Akhtar, Design, synthesis, and testing of high coercivity cobalt doped nickel ferrite nanoparticles for magnetic applications, J. Magn. Magn. Mater. 469 (2019) 674–680, https://doi.org/10.1016/j.jmmm.2018.09.021.

[55] X. Zuo, S. Yan, B. Barbiellini, V.G. Harris, C. Vittoria, A computational study of nickel ferrite, J. Magn. Magn. Mater. 303 (2006) e432–e435, https://doi.org/10.1016/j.jmmm.2006.01.102.

[56] X. Zeng, J. Zhang, M. Si, D. Cao, X. Deng, H. Ma, Q. Lan, D. Xue, X. Zhang, K. Tao, Y. Peng, Direct imaging of dopant sites in rare-earth element-doped permanent magnet and correlated magnetism origin, Nanoscale 11 (2019) 4385–4393, https://doi.org/10.1039/C8NR09922G.

[57] S.I. Ahmad, S.A. Ansari, D. Ravi Kumar, Structural, morphological, magnetic properties and cation distribution of Ce and Sm co-substituted nano crystalline cobalt ferrite, Mater. Chem. Phys. 208 (2018) 248–257, https://doi.org/10.1016/j.matchemphys.2018.01.050.

[58] G. Chai, N.N. Phuoc, C.K. Ong, Exchange coupling driven omnidirectional rotatable anisotropy in ferrite doped CoFe thin film, Sci. Rep. 2 (2012) 832, https://doi.org/10.1038/srep00832.

[59] I.O. Troyanchuk, S.V. Trukhanov, H. Szymczak, K. Baerner, Effect of oxygen content on the magnetic and transport properties of $Pr_{0.5}Ba_{0.5}MnO_{3-\gamma}$, J. Phys.: Condens. Matter 12 (2000) L155–L158, https://doi.org/10.1088/0953-8984/12/7/103.

[60] S.V. Trukhanov, I.O. Troyanchuk, A.V. Trukhanov, I.M. Fita, A.N. Vasil'ev, A. Maignan, H. Szymczak, Magnetic properties of La0.70Sr0.30MnO2.85 anion-deficient manganite under hydrostatic pressure, J. Exp. Theor. Phys. Lett. 83 (2006) 33–36, https://doi.org/10.1134/S0021364006010085.

[61] A.D. Bamburov, A.A. Markov, M.V. Patrakeev, I.A. Leonidov, The impact of Ba substitution in lanthanum-strontium ferrite on the mobility of charge carriers, Solid State Ion.-. 332 (2019) 86–92, https://doi.org/10.1016/j.ssi.2019.01.013.

[62] Jorge Andrés Chavarría-Rubio, Dora Alicia Cortés-Hernández, Andrés Manuel Garay-Tapia, Gilberto Francisco Hurtado-López, The role of lanthanum in the structural, magnetic and electronic properties of nanosized mixed manganese ferrites, J. Magn. Magn. Mater. 553 (2022) 169253, https://doi.org/10.1016/j.jmmm.2022.169253.

[63] M.A. Gabal, Y.M. Al Angari, A.Y. Obaid, A. Qusti, Structural analysis and magnetic properties of nanocrystalline NiCuZn ferrites synthesized via a novel gelatin method, Adv. Powder Technol. 25 (2014) 457–461, https://doi.org/10.1016/j.apt.2013.07.009.

[64] V. Sedykh, O. Rybchenko, V. Rusakov, S. Zaitsev, O. Barkalov, E. Postnova, T. Gubaidulina, D. Pchelina, V. Kulakov, Role of Fe atom valence states and oxygen vacancies in substituted lanthanum ferrite $La_{0.67}Sr_{0.33}FeO_{3-\gamma}$, J. Phys. Chem. Solids 171 (2022) 111001 https://doi.org/10.1016/j.jpcs.2022.111001.

[65] A. Ghasemi, Compositional dependence of magnetization reversal mechanism, magnetic interaction and Curie temperature of $Co_{1-x}Sr_xFe_2O_4$ spinel thin film, J. Alloy. Compd. 645 (2015) 467–477, https://doi.org/10.1016/j.jallcom.2015.05.013.

[66] Z. Xueyun, Y. Dongsheng, Z. Liling, Z. Lingling, Improved cut-off frequency in Gd/La doped NiZnCo ferrites, Mater. Sci. Eng. B. 272 (2021) 115334, https://doi.org/10.1016/j.mseb.2021.115334.

[67] A. Verma, R. Chatterjee, Effect of zinc concentration on the structural, electrical and magnetic properties of mixed Mn–Zn and Ni–Zn ferrites synthesized by the citrate precursor technique, J. Magn. Magn. Mater. 306 (2006) 313–320, https://doi.org/10.1016/j.jmmm.2006.03.033.

[68] Z. Peng, X. Fu, H. Ge, Z. Fu, C. Wang, L. Qi, H. Miao, Effect of Pr^{3+} doping on magnetic and dielectric properties of Ni–Zn ferrites by "one-step synthesis, J. Magn. Magn. Mater. 323 (2011) 2513–2518, https://doi.org/10.1016/j.jmmm.2011.05.033.

[69] S. Sankarrajan, K. Sakthipandi, P. Manivasakan, K. Thyagarajan, V. Rajendran, On-line phase transition in $La_{1-x}Sr_xMnO_3$ ($0.28 \leq x \leq 0.36$) perovskites through ultrasonic studies, Phase Transit. 84 (2011) 657–672, https://doi.org/10.1080/01411594.2011.556915.

[70] K. Sakthipandi, V. Rajendran, On-line phase transitions of bulk and nanocrystalline $La_{1-x}Pb_xMnO_3$ (x=0.3, 0.4, and 0.5) perovskite manganite materials using ultrasonic measurements, Mater. Chem. Phys. 138 (2013) 581–592, https://doi.org/10.1016/j.matchemphys.2012.12.023.

[71] S.A. Majetich, T. Wen, O.T. Mefford, Magnetic nanoparticles, MRS Bull. 38 (2013) 899–903, https://doi.org/10.1557/mrs.2013.230.

[72] C. Radhakrishnamurty, S.D. Likhite, Hopkinson effect, blocking temperature and Curie point in basalts, Earth Planet. Sci. Lett. 7 (1970) 389–396, https://doi.org/10.1016/0012-821X(70)90080-4.